Abdominal Radiology

Published online: 18 September 2018

Abdom Radiol (2019) 44:539–548
https://doi.org/10.1007/s00261-018-1768-9

Hepatocellular carcinoma: preoperative gadoxetic acid–enhanced MR imaging can predict early recurrence after curative resection using image features and texture analysis

Su Joa Ahn,[1] Jung Hoon Kim,[1,2] Sang Joon Park,[1] Seung Tack Kim,[1] and Joon Koo Han[1,2]

[1]Department of Radiology, Seoul National University Hospital, 101 Daehangno, Chongno-gu, Seoul 110-744, Korea
[2]Institute of Radiation Medicine, Seoul National University College of Medicine, Seoul, Korea

Abstract

Purpose: To investigate whether pre-operative gadoxetic acid–enhanced MRI can predict early recurrence after curative resection of single HCC using image features and texture analysis.

Materials and methods: 179 patients with single HCC and who underwent pre-operative MRI were included. Two reviewers analyzed MR findings, including the tumor margin, peritumoral enhancement, peritumoral hypointensity on the hepatobiliary phase (HBP), diffusion restriction, capsule, tumoral fat, washout, portal-vein thrombus, signal intensity on HBP, and satellite nodule. Texture analysis on the HBP was also quantified. A multivariate analysis was used to identify predictive factors for early recurrence, microvascular invasion (MVI), and the tumor grade.

Results: For early recurrence, satellite nodule, peritumoral hypointensity, absence of capsule, and GLCM ASM were predictors ($P < 0.05$). For MVI, satellite nodule, peritumoral hypointensity, washout, and sphericity were predictors ($P < 0.05$). Satellite nodules, peritumoral hypointensity, diffusion restriction, and iso to high signal intensity on HBP were predictor for higher tumor grade ($P < 0.05$). Satellite nodules and peritumoral hypointensity were important showed common predictors for early recurrence, MVI, and grade ($P < 0.05$). The sensitivity and specificity for satellite nodule were 47.36% and 96.25%. When added texture variables to MRI findings, the diagnostic performance for predicting early recurrence is improved from 0.7 (SD 0.604–0.790) to 0.83 (SD 0.787–0.894).

Conclusion: MR finding, including satellite nodule and peritumoral hypointensity on the HBP, as well as the texture parameters are useful to predict not only early recurrence, but also MVI and higher grade.

Key words: Hepatocellular carcinoma—Gadoxetic acid–enhanced MRI—Texture analysis—Recurrence—Microvascular invasion

Hepatocellular carcinoma (HCC) is the sixth most common cancer worldwide and one of the leading causes of cancer-related death [1]. Hepatic resection is the primary treatment modality for HCC in patients with well-preserved liver function [2, 3]. However, recurrence rates after hepatic resection can be as high as 50% within 5 years [4]. Of these rates, intra-hepatic distant recurrence (IDR) is associated with the worse prognosis and usually manifests as early recurrence within the first year after HCC resection [5, 6]. Given the general invasiveness of surgery and limited organ availability, it is important to identify patients who are most likely to experience a long-term curative outcome without recurrence. Therefore, the risk factors for early IDR after hepatic resection have been studied. Several published studies have found that early IDR is more likely to be associated with tumor factors such as tumor size, microvascular invasion, and a worse tumor grade [6–8].

Recently, magnetic resonance (MR) imaging has had an important role regarding the diagnosis and staging of the HCC. Recently, imaging findings, such as peritumoral parenchymal enhancement, an unsmooth tumor margin, and a lower apparent diffusion coefficient (ADC) value seen on the diffusion-weighted imaging

Correspondence to: Jung Hoon Kim; *email:* jhkim2008@gmail.com

(DWI), have been reported to be useful findings for predicting bad tumor behavior [9–11]. However, MR imaging still has limitations for predicting the tumor prognosis using imaging findings. Texture analysis is a quantitative image processing algorithm which can be used to quantify tissue heterogeneity by assessing the distribution of texture coarseness and irregularity within a lesion, and which is thus expected to allow a more detailed and reproducible quantitative assessment of lesion characteristics than visual analysis by human observers. Several published studies have assessed the potential of texture analysis to improve the prognostic information of current imaging and to confirm the hypothesis that greater tumor heterogeneity is an indicator of a poor clinical prognosis [12–15].

As far as we know, the value of a combination of imaging features and texture analysis using gadoxetic acid–enhanced MR imaging for the prediction of the early recurrence, microvascular invasion (MVI), and tumor grade of HCC after curative resection has not been studied. The purpose of this study is to investigate whether pre-operative, gadoxetic acid–enhanced MRI can predict the early recurrence, MVI, and tumor grade of a single HCC after curative resection with the use of image features and texture analysis.

Materials and methods

Patients

This retrospective study was approved by our institutional review board, and the requirement to obtain written, informed consent was waived. By searching our institution's database, we identified 294, consecutive patients who underwent curative hepatic resection for HCC at our institution between January 2012 and December 2013. Figure 1 summarizes the flowchart of the study. Finally, 179 patients who underwent curative hepatic resection (R0 resection) for a single HCC and who underwent pre-operative, gadoxetic acid–enhanced MR imaging were included in our study. The mean time interval between gadoxetic, acid–enhanced MR imaging and surgery was 15 ± 3 days.

Curative resection was defined as resection with a tumor-free margin and no residual tumors in the remnant liver, and early recurrence (ER) was defined as recurrence within the first year after HCC resection. The medical records of all patients were reviewed retrospectively, and data for demographics, laboratory results including tumor markers, tumor pathology, and recurrence were collected for each patient. Pathology data revealed the presence of microvascular invasion. Satellite nodules were defined as microscopic HCC nodules separated from the main tumor. The tumor grade was classified as low grade and high grade using Edmondson and Steiner grading system [16]. Tumor grades I and II belonged to the low-grade group, and tumor grades III and IV belonged to the high-grade group. For follow-up after surgery, patients were followed in the outpatient clinic every 3 months for the first 2 years and every 6 months thereafter. We evaluated recurrence on the basis of laboratory measurements including alpha-fetoprotein (AFP) and prothrombin induced by vitamin K absence or antagonist-II (PIVKA-II) and dynamic computed tomography or magnetic resonance imaging at each visit. Recurrence was defined as the appearance of a new lesion compatible with HCC on radiologic examination during the follow-up period or pathologic result according percutaneous liver biopsy or additional surgery.

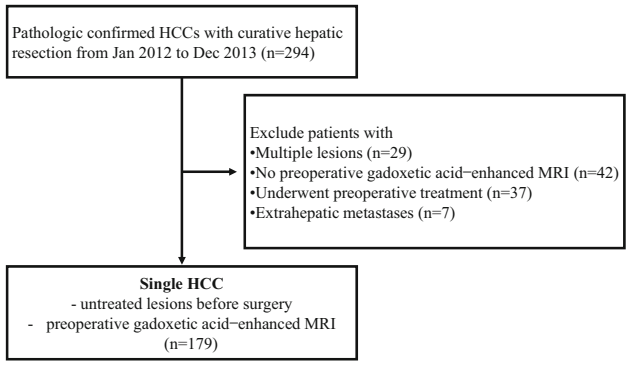

Fig. 1. Flowchart shows study group inclusion process. Numbers in parentheses are numbers of patients. HCC: Hepatocellular carcinoma, MRI: magnetic resonance imaging.

MR techniques

MR examinations were performed using 1.5 T MR scanners (Signa Excite, GE Medical Systems, Milwaukee, WI, USA, $n = 90$) and 3T MR scanners (Magnetom Verio or Magnetom Trio, Siemens Healthcare, Erlangen, Germany, $n = 50$; Ingenia, Philips Medical System, Best, Netherlands, $n = 39$). Our liver MRI protocol consisted of a breath-hold, fat-saturated, T2-weighted, fast spin echo or turbo spin echo (TSE) sequence, a breath-hold, T1-weighted, dual-echo (in-phase and opposed-phase) gradient-echo (GRE) sequence, dynamic, 3D fat-saturated, T1-weighted GRE sequences, and free-breathing DWI using a single-shot echo-planar imaging sequence. Dynamic 3D fat-saturated, T1-weighted GRE sequences were performed both before and after administration of contrast medium (gadoxetic acid, Primovist ®, Bayer Healthcare, Berlin, Germany). All of the patients received a rapid bolus of 1 mL/10 kg per body weight (0.025 mmol/kg) of gadoxetic acid at a rate of 1.5 mL/s, immediately followed by a 30-mL saline flush through an antecubital venous catheter and using a power injector (Spectris Solaris EP, MEDRAD Inc., Warrendale, PA,

Table 1. Baseline demographic characteristics of the study populations

Characteristics	Early recurrence				Microvascular invasion				Tumor grade			
	Absent (n = 141)	Present (n = 38)	Total (n = 179)	P value[a]	Absent (n = 111)	Present (n = 68)	Total (n = 179)	P value[a]	Low grade (n = 91)	High grade (n = 88)	Total (n = 179)	P value[a]
Sex (Male/female)	118/23	29/9	147/32	0.55	92/19	55/13	147/32	0.86	75/16	71/17	147/32	0.77
Age (years)	55.49 (29–79)	61.25 (36–85)	56.71 (29–85)	0.12	57.63 (35–79)	57.35 (29–85)	56.71 (29–85)	0.90	58.89 (29–78)	56.11 (29–85)	56.71 (29–85)	0.08
Etiology (Alcohol/HBV/HCV/ HBV&HCV/idiopathic)	4/116/6/1/14	2/31/3/0/2	6/147/9/1/ 16	0.24	3/92/5/1/10	3/55/4/0/6	6/147/9/1/ 16	0.55	3/71/4/1/2	3/76/5/0/4	6/147/9/1/ 16	0.31
Child–Pugh class (A/B)	139/2	37/1	176/3	0.65	109/2	67/1	176/3	0.79	90/1	86/2	176/3	0.74
AFP (ng/mL)[b]	13.92 ± 0.92	12.32 ± 0.69		0.12	9.38 ± 0.62	15.81 ± 0.28		0.04	12.92 ± 0.62	13.90 ± 0.41		0.13
PIVKA-II (mAU/mL)[b]	37.76 ± 0.91	36.21 ± 0.66		0.35	24.14 ± 0.23	43.91 ± 0.28		< 0.01	37.51 ± 0.55	38.23 ± 0.52		0.17
Local staging[c] (T1a/T1b/T2)	36/68/37	5/12/21	41/80/58	0.05	40/71/5	1/9/53	41/80/58	< 0.01	35/58/21	6/22/37	41/80/58	0.04
Microvascular invasion	46	22	68	< 0.01					73/18	38/50	68	< 0.01
Tumor grade (GI + II/ GIII + IV)	63/78	28/10	91/88	< 0.01	73/38	18/50	91/88	< 0.01				
Early recurrence					95/16	46/22	141/38	< 0.01	82/9	59/29	91/88	< 0.01
Surgical treatment (Local excision/Liver transplantation)	140/1	38/0	178/1	0.77	110/1	68/0	178/1	0.82	90/1	88/0	178/1	0.61

HBV Chronic hepatitis B, *HCV* Chronic hepatitis C

[a] χ^2 test

[b] Mean age ± standard deviation (range)

[c] TNM staging

USA). The arterial phase was scanned seven seconds after the contrast media had arrived at the distal thoracic aorta, and the portal venous phase, transitional phase, and hepatobiliary phase (HBP) images were subsequently obtained 50 s, 3 and 20 min, respectively, after starting the contrast medium injection. The detailed scanning parameters of the MR equipment used are summarized in Table 5 in Appendix. Subsequently, DWIs were obtained using a free-breathing, single-shot echo-planar imaging pulse sequence with diffusion gradients applied in three, orthogonal directions and using b values of 0, 100, and 800 mm^2/s. ADC maps were automatically generated on a pixel-by-pixel basis.

Image analysis

Two radiologists (JH Kim and ST Kim with 17 and 5 years, respectively, of clinical experience in abdominal MR imaging) who were blinded to the clinical, laboratory, and pathology information, independently determined whether the following imaging features were present or absence in each HCC: (a) peritumoral parenchymal enhancement in the arterial phase, defined as grossly hyperarterial contrast material enhancement outside of the tumor border that becomes isointense with background liver parenchyma in the later dynamic phase images, regardless of shape (e.g., wedge shaped or circumferential); (b) capsule, defined as a distinct, low-signal-intensity ring with enhancement along the tumor border; (c) peritumoral hypointensity in the HBP, defined as an irregular, wedge-shaped, or flamelike area of low signal intensity in the liver parenchyma located outside of the tumor margin in the hepatobiliary phase [17]; (d) non-smooth tumor margin in the HBP and which is considered to be present in a multinodular confluent, nodular with extranodular extension, and/or infiltrative shaped tumor; (e) satellite nodules which are lesions as satellites were defined as tumors ≤ 2 cm in size and located ≤ 2 cm from the main tumor [18]; (f) intratumoral fat; (g) intra–hepatic, portal-vein thrombus; (h) washout, defined as the arterial-enhanced portion of the tumor changed to lower signal than the surrounding liver tissue seen on the portal phase; (i) HBP signal intensity; and (j) diffusion restriction with a high b value (800 s/mm^2). When there was a discrepancy between the two radiologists' diagnoses, the third reviewer JK Han made the final decision. One radiologist (AJ Ahn) measured the tumor size, defined as the maximum diameter of each tumor as measured using the electronic caliper on the picture-archiving and communication system.

Computerized texture analysis

The HBP images were retrieved from our institution's archive and were loaded onto a standard workstation for further texture analysis. Our personal, computer–based, in-house software program (Medical Imaging Solution for Segmentation and Texture Analysis) was used for lesion segmentation with fully automated quantification of texture features implemented using a dedicated C++ language (Microsoft Foundation Classes; Microsoft, Redmond, WA, USA). Image examples are shown in Fig. 2. Prior to performing texture analysis, two radiologists (JH Kim and SJ Ahn with 17 and 5 years, respectively, of experience in abdominal MR imaging) reviewed the HBP images and selected in consensus the most representative HCC image plan. One radiologist (AJ Ahn) then performed segmentation of the HCC by manually drawing a region of interest around the outline using the texture analysis software program. For tumor texture analysis, a region of interest was initially delineated around the tumor outline in order to show the largest cross-sectional area in a single HCC and texture features were then automatically calculated. Analyzed texture features included histogram features and morphologic features. The histogram parameters analyzed included mean attenuation, standard deviation, skewness (skewness of the pixel distribution), kurtosis (magnitude of the pixel distribution), entropy (irregularity), and homogeneity. The following morphologic and texture features were then obtained: sphericity; discrete compactness; gray-level co-occurrence matrix (GLCM) moments; the GLCM angular second moment (ASM)*; the GLCM* inverse difference moment *(IDM); GLCM contrast; and GLCM entropy*.

Statistical analysis

In order to compare the presence and absence of early recurrence, MVI, and a different tumor grade, we used the Student *t*, the Mann–Whitney *U* test, the cui-square, or Fisher exact test. The cui-square or Fisher's exact test was used to examine the relationships between pathology and image findings. Logistic regression analysis was performed in order to identify significant predictors. First, univariate analysis was performed for each image finding and texture parameter, and only variables with *P*-values < 0.05 were selected as input variables for multivariate analysis. Receiver–operating characteristics analysis was used for single predicting variables as well as for regression equations in order to evaluate their diagnostic ability of early recurrence. Inter-observer agreement was evaluated using the Cohen k coefficient. A k statistic of 0.8–1 was considered to indicate excellent agreement; 0.6–0.79, good agreement; 0.4–0.59, moderate agreement; 0.2–0.39, fair agreement; and 0–0.19, poor agreement. Two-sided $P < 0.05$ was considered to indicate a statistically significant difference. All analyses were performed by using the software SPSS version 18.0; SPSS, Chicago, IL, USA or MedCalc for Windows, version 16.8.4; Med Calc Software, Mariakerke, Belgium).

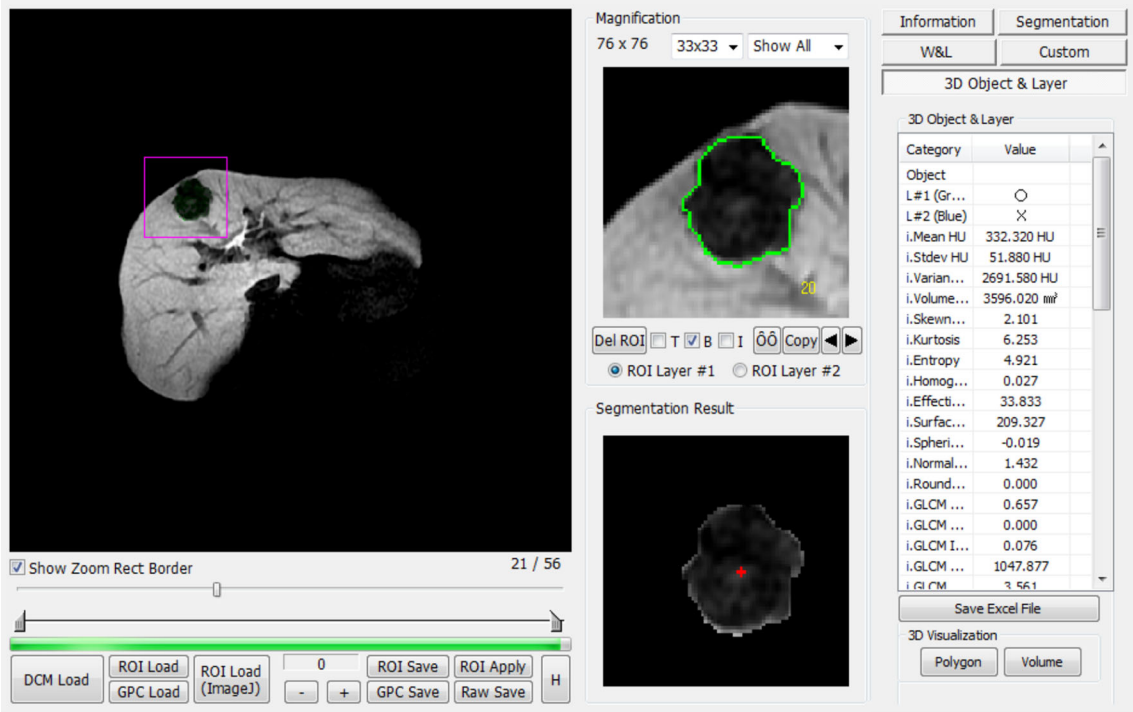

Fig. 2. CT texture analysis software program. The segmentation of hepatic metastasis was manually conducted by using an in-house software program and texture features of the nodules were automatically extracted and calculated by the software program.

Results

Early recurrence after curative resection of HCC was found in 38 patients (38/179, 21%, Table 1). 33 patients were diagnosed with image finding and residual 5 patients diagnosed with pathology. The mean time to early recurrence was 9 ± 6.4 months (range 1–11 months). Sixty-eight patients had MVI ($n = 68/179$, 38%). Low-grade HCC (grade I = 12 and II = 79) was found in 91 patients ($n = 91/179$, 50.8%), and high-grade HCC (grade III = 76 and IV = 12) was found in 88 patients ($n = 88/179$, 49.2%). In patients with early recurrence, significantly more MVI was observed (59.9%, 22/38) than in patients with non-early recurrence (32.6%, 46/141, $P = 0.004$), and high-grade HCC was more commonly observed in the early recurrence group (3.42 ± 0.43) than in the non-early recurrence group (2.76 ± 0.49) ($P < 0.001$).

Common MR findings of early recurrence, MVI, and a higher tumor grade

The common findings of early recurrence included a non-smooth tumor margin, peritumoral parenchymal enhancement, peritumoral hypointensity on the HBP, the absence of a radiologic capsule, satellite nodules, and portal-vein thrombus ($P < 0.05$). MVI was significantly associated with larger tumor size, a non-smooth tumor margin, peritumoral hypointensity on the HBP, washout, portal-vein thrombus, and a satellite nodule ($P < 0.05$). High tumor grade was significantly associated with peritumoral enhancement, peritumoral hypointensity on the HBP, diffusion restriction, hypointensity on the HBP, and satellite nodules ($P < 0.05$). Peritumoral hypointensity and satellite nodules revealed significant findings in early recurrence, MVI, and high tumor grade. Table 2 summarizes the common findings of early recurrence, MVI, and high tumor grade. Each MRI finding showed good or excellent inter-observer agreement ($k = 0.69$–0.87).

Common texture variables of early recurrence, MVI, and high tumor grade

The texture analysis variables for the prediction of early recurrence included entropy, GLCM ASM, and GLCM Entropy ($P < 0.05$). In MVI, the significant texture features included sphericity and discrete compactness ($P < 0.05$). However, there were no significant, associated texture variables in high tumor grade (Table 3, Fig. 3).

Important MR findings and texture variables for predicting early recurrence, MVI, and high tumor grade

Table 4 summarizes the MR findings and texture variables used to predict the early recurrence of HCC, MVI, and high tumor grade. Both peritumoral hypointensity

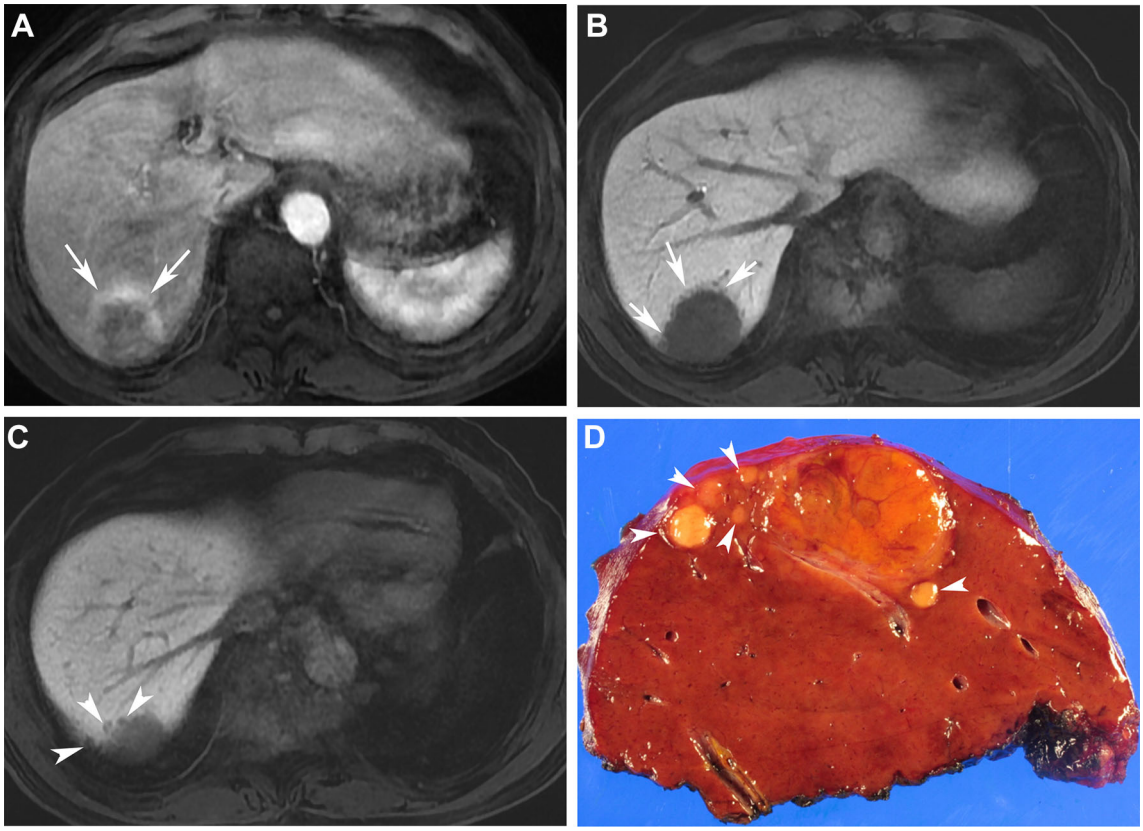

Fig. 3. A 73-year-old man with a 4.5 cm HCC with high tumor grade (Edmondson and Steiner's grade III) and microvascular invasion. Arterial phase MR image (**A**) shows a 4.5 cm mass in segment VII of the liver. Peritumoral enhancement in the arterial phase is noted (arrows). HBP MR images (**B**, **C**) show peritumoral hypointensity (arrows) and three satellite nodules (arrowheads). The GLCM ASM of the mass on the HBP was 0.001. Gross specimen (**D**) reveals five satellite nodules (arrowheads).

Table 2. Common MRI findings of early recurrence, microvascular invasion, and high tumor grade

MRI findings	Early recurrence			Microvascular invasion			Tumor grade			Kappa value
	Absent (n = 141, %)	Present (n = 38, %)	P value	Absent (n = 111, %)	Present (n = 68, %)	P value	Low grade (n = 91, %)	High grade (n = 88, %)	P value	
MR size (mm)	40.9 ± 26.8	54.0 ± 37.5	0.05	38.1 ± 26.1	52.7 ± 33.2	< 0.01	42.5 ± 27.7	44.9 ± 31.9	0.59	0.78
Margin_non smooth	65 (46)	27 (71)	< 0.01	46 (41)	46 (68)	< 0.01	41 (45)	51 (58)	0.08	0.73
Peritumoral enhancement	44 (31)	20 (53)	0.01	33 (30)	31 (46)	0.37	25 (27)	39 (44)	0.02	0.79
Peritumoral hypointensity	40 (28)	21 (55)	< 0.01	26 (23)	35 (51)	< 0.01	23 (25)	38 (43)	0.01	0.76
Diffusion restriction	134 (95)	37 (97)	0.54	105 (95)	6 (9)	0.49	84 (92)	87 (99)	0.03	0.87
Radiologic capsule	97 (69)	17 (45)	< 0.01	68 (61)	46 (68)	0.46	64 (70)	50 (57)	0.06	0.77
Hypo SI on HBP	16 (11)	1 (3)	0.10	11 (10)	6 (9)	1	13 (14)	88 (100)	0.03	0.73
Intratumoral fat	40 (28)	13 (34)	0.48	33 (30)	20 (29)	1	32 (35)	21 (24)	0.10	0.78
Washout	110 (78)	31 (82)	0.63	80 (72)	61 (90)	< 0.01	67 (74)	74 (84)	0.09	0.69
PVT	4 (3)	5 (13)	0.01	5 (5)	4 (6)	< 0.01	2 (2)	7 (8)	0.08	0.72
Satellite nodule	7 (5)	8 (21)	< 0.01	3 (3)	12 (18)	< 0.01	3 (3)	12 (14)	< 0.01	0.74

Independent sample t- test
PVT, portal vein thrombus

Table 3. Comparison of texture variable of HCC in early recurrence, microvascular invasion, tumor grade

Texture variables	Early recurrence			Microscopic vessel invasion			Tumor grade		
	Absent (n = 141)	Present (n = 38)	P value	Absent (n = 111)	Present (n = 68)	P value	Low grade (n = 91)	High grade (n = 88)	P value
Mean attenuation (HU)	351.27 ± 344.84	381.70 ± 374.68	0.64	366.81 ± 363.23	342.89 ± 330.83	0.66	358.66 ± 393.85	356.77 ± 301.53	0.97
Standard deviation (HU)	48.07 ± 55.11	55.66 ± 47.86	0.44	50.17 ± 57.74	48.87 ± 46.48	0.88	49.42 ± 64.17	49.95 ± 40.30	0.95
Skewness	0.78 ± 0.81	0.81 ± 0.62	0.70	0.66 ± 0.89	0.71 ± 0.65	0.68	0.57 ± 0.87	0.79 ± 0.73	0.06
Kurtosis	1.83 ± 2.32	1.74 ± 1.97	0.83	1.87 ± 2.53	1.70 ± 1.69	0.60	1.71 ± 2.40	1.92 ± 2.09	0.53
Entropy	4.64 ± 0.69	4.91 ± 0.69	0.03	4.68 ± 0.68	4.72 ± 0.71	0.69	4.66 ± 0.71	4.73 ± 0.68	0.49
Homogeneity	0.02 ± 0.018	0.022 ± 0.013	0.88	0.02 ± 0.02	0.02 ± 0.02	0.99	0.02 ± 0.02	0.02 ± 0.01	0.89
Sphericity	− 1.36 ± 0.66	− 1.58 ± 0.81	0.14	− 1.28 ± 0.63	− 1.61 ± 0.76	< 0.01	− 1.40 ± 0.67	− 1.42 ± 0.74	0.86
Discrete Compactness	1.75 ± 0.28	1.66 ± 0.26	0.08	1.78 ± 0.29	1.65 ± 0.21	< 0.01	1.76 ± 0.31	1.70 ± 0.24	0.14
GLCM Moments	1.86 ± 0.94	1.86 ± 0.85	0.99	1.86 ± 0.92	1.86 ± 0.92	0.98	1.85 ± 0.87	1.87 ± 0.97	0.86
GLCM ASM	0.03 ± 0.01	0.01 ± 0.01	0.01	0.01 ± 0.01	0.01 ± 0.01	0.41	0.01 ± 0.01	0.01 ± 0.01	0.49
GLCM IDM	0.10 ± 0.06	0.08 ± 0.04	0.12	0.89 ± 0.06	0.10 ± 0.06	0.11	0.10 ± 0.06	0.09 ± 0.06	0.82
GLCM Contrast	1130.94 ± 2064.07	1079.03 ± 1584.46	0.88	1160.25 ± 1943.59	1054.09 ± 2020.13	0.73	1032.93 ± 2007.49	1209.88 ± 1933.747	0.55
GLCM Entropy	3.36 ± 0.40	3.56 ± 0.41	0.01	3.37 ± 0.41	3.46 ± 0.41	0.18	3.38 ± 0.41	3.43 ± 0.42	0.42

Except where indicated, data are mean ± standard deviation
Independent sample t- test
GLCM, gray-level values in the matrix; GLCM ASM, angular second moment; GLCM IDM, inverse difference moment

on the HBP and the presence of a satellite nodule were significant independent predictors ($P < 0.05$); peritumoral hypointensity and the presence of a satellite nodule in early recurrence; peritumoral hypointensity and the presence of a satellite nodule for MVI; and peritumoral hypointensity and the presence of satellite nodules for a high tumor grade. The sensitivity, specificity, PPV, and NPV for satellite nodule detection on MRI were 47.36%, 96.25%, 60%, and 93.9%, respectively.

Diagnostic performance of MRI findings and texture variables for predicting the early recurrence of HCC

Using the MRI findings, including the presence of a satellite nodule, non-smooth tumor margin, peritumoral enhancement, peritumoral hypointensity, and the absence of a radiologic capsule, the diagnostic performance for predicting early recurrence was 0.7 (SD 0.604–0.790). When we apply both MR findings and texture variables including entropy, GLCM ASM, and GLCM Entropy, the diagnostic performance for predicting early recurrence was improved up to 0.83 (SD 0.787–0.894).

Discussion

Early recurrence after surgical resection of HCC varied from 20.8% to 44% [19, 20]. Therefore, the pre-operative risk stratification of early recurrence is important for determining the best candidates for surgical resection. MVI and higher tumor grade are also important factors not only for predicting early recurrence, but also for assessing long-term patient survival [21, 22]. In our study early recurrence was noted in 21.2% (38 of 179) and that rate correlates well with that seen in previous studies [19, 20]. In our study, MVI (59.9%, 22/38, $P = 0.004$) and a high tumor grade (26.3%, 10/38, $P < 0.001$) were significantly higher in the early recurrence group. Both peritumoral hypointensity on the HBP and the presence of satellite nodules were significant independent predictors of the early recurrence, MVI, and high tumor grade. When we apply both MR findings and texture variables, the diagnostic performance for prediction of early recurrence was improved to 0.83 from 0.72.

According to previous reports, MR findings including a non-smooth tumor [10], washout [23], peritumoral hypointensity on the HBP [19], a pseudocapsule [24], and the ADC value [11] are important for the prediction of early recurrence, MVI, and a high tumor grade. In our study, peritumoral hypointensity and satellite nodules were significant findings for predicting early recurrence, MVI, and a high tumor grade ($P < 0.05$). Kim et al. [17] reported that the peritumoral hypointensity showed high specificity (93.2%) and a PPV of 88.5% for MVI in 104 patients with HCC. They explained that these results were caused by decreased uptake of gadoxetate disodium

Table 4. Important MR findings and texture analysis variables to predict early recurrence, microvascular invasion, and high tumor grade

	Variable	Adjusted odds ratio	*P* value
Early recurrence	Peritumoral hypointensity	2.921 (1.343, 1.030)	0.007
	Absence of radiologic capsule	2.86 (0.763, 0.161)	0.008
	Satellite nodule	4.7 (1.426, 15.495)	0.011
	GLCM ASM	2.389 (0.915, 6.240)	0.04
Microvascular invasion	Peritumoral hypointensity	2.99 (1.480, 6.040)	0.002
	Washout	4.316 (1.558, 11.953)	0.005
	Satellite nodule	7.972 (1.839, 34.563)	0.006
	Sphericity	0.499 (0.316, 0.788)	0.003
High tumor grade	Peritumoral hypointensity	1.857 (0.960, 3.593)	0.031
	HBP SI_iso/high	0.281 (0.086, 0.920)	0.048
	Diffusion restriction	5.894 (0.698, 49.789)	0.041
	Satellite nodule	3.983 (1.039, 6.356)	0.044

Data are adjusted odds ratios per one standard deviation change; data in parentheses are 95% confidence intervals

by hepatocytes caused by obstruction of minute, portal branches by tumor thrombi, and resulting in hemodynamic changes. Choi et al. [25] also determined that if the intra-hepatic portal vein is occluded and hepatic arterial flow is insufficiently compensated, the liver parenchyma is injured, and thus causing edema, hepatocytic depletion, and fibrosis that may result in peritumoral hypointensity. As mentioned above, perfusion changes by MVI of HCC may affect the organic anion transporting peptides or the canalicular transporter multidrug resistance-associated protein 2 within hepatocytes, and which are known to cause the uptake of gadoxetate disodium [26, 27]. In our study, peritumoral hypointensity on the HBP showed a significant prediction of early recurrence, MVI, and high tumor grade.

In our study, the presence of a satellite nodule also had a significant prediction of early recurrence, MVI and a high tumor grade. According to previously published reports, the presence of satellite nodules was a significant predictive factor for recurrence. Plessier et al. [28] reported that in 28 patients who had satellite nodules, seven had recurrence, whereas in 41 patients who did not have satellite nodules, no recurrence developed and that the presence of satellite nodules was the only significant predictive factor for recurrence after liver transplantation ($P < 0.001$) and was also significantly correlated with MVI ($P = 0.002$). And Pesi et al. [29] found that the disease-free survival after liver resection for HCC at one, three and five years in patients with and without satellite nodules was 84%, 34%, and 25% vs. 90%, 64%, and 46%, respectively ($P = 0.01$). Those results suggest that development of satellite nodules favors vascular invasion and also tumor recurrence. Gadoxetic acid–enhanced MRI provides high specificity for the detection of satellite nodules. In our study, the specificity and NPV for satellite nodules were 96.25%, and 93.9%, respectively.

Even though MRI findings are important for the prediction of early recurrence, texture analysis may be useful for improving the diagnostic performance of MRI. In our study, the diagnostic performance for the prediction of early recurrence was improved up to 0.83 from 0.72 when we applied both MR findings and texture variables. Investigations of texture analysis for early detection of liver malignancy have shown promising results using CT images. Ganeshan et al. found that the diagnostic performance of entropy for the diagnosis of liver metastasis was 0.802($P < 0.0005$) in 32 patients [30] and that the gray-level distribution performed well for detecting malignancies and with an 81.7% accuracy for classifying malignancies in the 80 malignant liver tumors [31]. However, there have only been few studies regarding the texture analysis of HCC. Zhou et al. [32] studied the use of gadoxetic acid-enhanced MRI data regarding 46 consecutive patients with resected HCC in order to determine the performance of texture features for differentiating the tumor grade. They concluded that texture features indexed by a lower mean intensity value and gray-level, run-length non-uniformity in the arterial phase proved to be associated with a high grade. In our study, lower GLCM ASM was significantly associated with early recurrence. That result was well-correlated with those of previous studies because the GLCM ASM measures the local uniformity of the gray levels [33]. When pixels differ, the ASM value will be small [33]. Therefore, small GLCM ASM indicates locally heterogeneity which is a well-recognized feature of malignancy that reflects areas of high cell density, necrosis, hemorrhage, and myxoid change [34].

Our study has several limitations. First, it was a retrospective study which means that it is subject to potential bias. We also used three, different MR scanners. Even though, this is also a potential bias, we acquired data using the standard liver MRI protocol. Second, as the texture variables in this study were derived from the results of manual segmentation by a radiologist, these results can be significantly influenced by a subjective tendency or bias on the part of the observers. However, manual segmentation is the current reference standard for lesion segmentation, particularly in the case

of infiltrative lesions as their margins are often indistinct from the normal hepatic parenchyma and therefore not technically easy to automatically segment. Nevertheless, we believe that a reliable and robust automatic boundary extraction method should be further developed in order to address the variability issue. Finally, in our study, we used 2D texture analysis. Even though, 2D texture analysis is more common than 3D texture analysis in the previous published studies, theoretically, whole tumor analysis is better than 2D analysis. In future work, we need to investigate whole tumor texture analysis.

When we plan curative surgical resection of an HCC, risk stratification of the individual risk of early tumor recurrence using pre-operative MRI findings and texture analysis can be used to tailor the management. In our study results, MRI findings, including peritumoral hypointensity and satellite nodules, were independent predictors for early recurrence, MVI, and high tumor grade after curative resection of a single HCC. In this study, when we applied both MRI findings and texture variables, the diagnostic performance for the prediction of early recurrence was improved. Further clinical and technical validations of this texture analysis need to be carried out in order to confirm these results.

Acknowledgments We also thank Bonnie Hami, M.A. (USA) for her editorial assistance in the preparation of this manuscript.

Compliance with ethical standards

Funding No funding.

Conflict of interest All authors confirm that no disclosure of potential conflicts of interest.

Ethical approval This retrospective study was approved by our institutional review board, and the requirement to obtain written, informed consent was waived.

Appendix

See Table 5.

Table 5. MR imaging parameters

Sequence[a]	Field strength (T)[b]	FOV (mm)	Slice thickness (mm)	Intersection Gap (mm)	TR/TE (msec)	Flip angle (degrees)	Matrix
Dual-echo T1-weighted GRE	1.5 (Signa Excite HD)	350 × 350	6	3	7.9/2.3	12	320 × 192
	3.0 (Magnetom Verio)	400 × 400	3	0	4.4/1.3	9	320 × 256
	3.0 (Magnetom Trio)	380 × 380	3	0	4.5/1.3	9	320 × 256
	3.0 (Ingenia)	410 × 410	6	3	4.3/2.3	10	368 × 299
T1-weighted 3D GRE	1.5 (Signa Excite HD)	380 × 380	6	3	4.5/2.2	12	320 × 224
	3.0 (Magnetom Verio)	400 × 400	3	0	3.5/1.3	11	384 × 278
	3.0 (Magnetom Trio)	380 × 380	3.2	0	3.4/1.3	11	384 × 292
	3.0 (Ingenia)	410 × 410	6	3	4.3 × 0.0	10	368 × 299
Diffusion-weighted imaging	1.5 (Signa Excite HD)	380 × 380	5	6	4500/64.6	90	128 × 96
	3.0 (Magnetom Verio)	400 × 400	7	7	2100/61	90	128 × 128
	3.0 (Magnetom Trio)	380 × 380	6	6.6	3000/63	180	128 × 128
	3.0 (Ingenia)	410 × 410	7	7	1427.7/69.4	90	128 × 104

[a]GRE, gradient-recalled echo; 3D, three-dimensional; TSE, turbo spin echo
[b]Trade name is in parentheses

References

1. Siegel RL, Miller KD, Jemal A (2017) Cancer statistics, 2017. CA Cancer J Clin 67:7–30
2. Roayaie S, Obeidat K, Sposito C, et al. (2013) Resection of hepatocellular cancer ≤ 2 cm: results from two Western centers. Hepatology 57:1426–1435
3. Omata M, Cheng AL, Kokudo N, et al. (2017) Asia-Pacific clinical practice guidelines on the management of hepatocellular carcinoma: a 2017 update. Hepatol Int 11:317-370
4. Shah SA, Cleary SP, Wei AC, et al. (2007) Recurrence after liver resection for hepatocellular carcinoma: risk factors, treatment, and outcomes. Surgery 141:330-339
5. Choi GH, Kim DH, Kang CM, et al. (2008) Prognostic factors and optimal treatment strategy for intrahepatic nodular recurrence after curative resection of hepatocellular carcinoma. Ann Surg Oncol 15:618–629
6. Poon RT, Fan ST, Ng IO, et al. (2000) Different risk factors and prognosis for early and late intrahepatic recurrence after resection of hepatocellular carcinoma. Cancer 89:500–507
7. Portolani N, Coniglio A, Ghidoni S, et al. (2006) Early and late recurrence after liver resection for hepatocellular carcinoma: prognostic and therapeutic implications. Ann Surg 243:229–235
8. Kamiyama T, Nakanishi K, Yokoo H, et al. (2012) Analysis of the risk factors for early death due to disease recurrence or progression within 1 year after hepatectomy in patients with hepatocellular carcinoma. World J Surg Oncol 10:107
9. Kim H, Park MS, Choi JY, et al. (2009) Can microvessel invasion of hepatocellular carcinoma be predicted by pre-operative MRI? Eur Radiol 19:1744–1751
10. Ariizumi S, Kitagawa K, Kotera Y, et al. (2011) A non-smooth tumor margin in the hepatobiliary phase of gadoxetic acid disodium (Gd-EOB-DTPA)-enhanced magnetic resonance imaging predicts microscopic portal vein invasion, intrahepatic metastasis, and early recurrence after hepatectomy in patients with hepatocellular carcinoma. J Hepatobiliary Pancreat Sci 18:575–585
11. Suh YJ, Kim MJ, Choi JY, Park MS, Kim KW (2012) Preoperative prediction of the microvascular invasion of hepatocellular carcinoma with diffusion-weighted imaging. Liver Transpl 18:1171–1178
12. Ganeshan B, Skogen K, Pressney I, Coutroubis D, Miles K (2012) Tumour heterogeneity in oesophageal cancer assessed by CT texture analysis: preliminary evidence of an association with tumour metabolism, stage, and survival. Clin Radiol 67:157–164
13. Ganeshan B, Miles KA, Young RC, Chatwin CR (2007) In search of biologic correlates for liver texture on portal-phase CT. Acad Radiol 14:1058–1068
14. Miles KA, Ganeshan B, Griffiths MR, Young RC, Chatwin CR (2009) Colorectal cancer: texture analysis of portal phase hepatic CT images as a potential marker of survival. Radiology 250:444–452
15. Ganeshan B, Panayiotou E, Burnand K, Dizdarevic S, Miles K (2012) Tumour heterogeneity in non-small cell lung carcinoma assessed by CT texture analysis: a potential marker of survival. Eur Radiol 22:796–802
16. Edmondson HA, Steiner PE (1954) Primary carcinoma of the liver. A study of 100 cases among 48,900 necropsies. Cancer 7:462-503
17. Kim KA, Kim MJ, Jeon HM, et al. (2012) Prediction of microvascular invasion of hepatocellular carcinoma: usefulness of peritumoral hypointensity seen on gadoxetate disodium-enhanced hepatobiliary phase images. J Magn Reson Imaging 35:629–634
18. Roayaie S, Blume IN, Thung SN, et al. (2009) A system of classifying microvascular invasion to predict outcome after resection in patients with hepatocellular carcinoma. Gastroenterology 137:850–855
19. Chong CC, Lee KF, Ip PC, et al. (2012) Pre-operative predictors of post-hepatectomy recurrence of hepatocellular carcinoma: can we predict earlier? Surgeon 10:260–266
20. Park UJ, Kim YH, Kang KJ, Lim TJ (2008) Risk factors for early recurrence after surgical resection for hepatocellular carcinoma. Korean J Hepatol 14:371–380
21. Sumie S, Kuromatsu R, Okuda K, et al. (2008) Microvascular invasion in patients with hepatocellular carcinoma and its predictable clinicopathological factors. Ann Surg Oncol 15:1375–1382
22. Lauwers GY, Terris B, Balis UJ, et al. (2002) Prognostic histologic indicators of curatively resected hepatocellular carcinomas: a multiinstitutional analysis of 425 patients with definition of a histologic prognostic index. Am J Surg Pathol 26:25–34
23. Griffin N, Addley H, Sala E, et al. (2012) Vascular invasion in hepatocellular carcinoma: is there a correlation with MRI? Br J Radiol 85:736–744
24. Ishigami K, Yoshimitsu K, Nishihara Y, et al. (2009) Hepatocellular carcinoma with a pseudocapsule on gadolinium-enhanced MR images: correlation with histopathologic findings. Radiology 250:435–443
25. Choi BI, Lee KH, Han JK, Lee JM (2002) Hepatic arterioportal shunts: dynamic CT and MR features. Korean J Radiol 3:1–15
26. Tsuboyama T, Onishi H, Kim T, et al. (2010) Hepatocellular carcinoma: hepatocyte-selective enhancement at gadoxetic acid-enhanced MR imaging-correlation with expression of sinusoidal and canalicular transporters and bile accumulation. Radiology 255:824–833
27. Kitao A, Zen Y, Matsui O, et al. (2010) Hepatocellular carcinoma: signal intensity at gadoxetic acid-enhanced MR imaging-correlation with molecular transporters and histopathologic features. Radiology 256:817–826
28. Plessier A, Codes L, Consigny Y, et al. (2004) Underestimation of the influence of satellite nodules as a risk factor for post-transplantation recurrence in patients with small hepatocellular carcinoma. Liver Transpl 10:S86–90
29. Pesi B, Moraldi L, Zambonin D, et al. (2014) Vascular invasion, satellite nodules and absence of tumor capsule strongly correlate with disease-free survival and long-term outcome in patients resected for hepatocellular carcinoma. J Cancer Ther 5:1344–1353
30. Ganeshan B, Miles KA, Young RC, Chatwin CR (2009) Texture analysis in non-contrast enhanced CT: impact of malignancy on texture in apparently disease-free areas of the liver. Eur J Radiol 70:101–110
31. Huang YL, Chen JH, Shen WC (2006) Diagnosis of hepatic tumors with texture analysis in nonenhanced computed tomography images. Acad Radiol 13:713–720
32. Zhou W, Zhang L, Wang K, et al. (2017) Malignancy characterization of hepatocellular carcinomas based on texture analysis of contrast-enhanced MR images. J Magn Reson Imaging 45(5):1476–1484
33. Zayed N, Elnemr HA (2015) Statistical analysis of haralick texture features to discriminate lung abnormalities. Int J Biomed Imaging 2015:267807
34. Nelson DA, Tan TT, Rabson AB, et al. (2004) Hypoxia and defective apoptosis drive genomic instability and tumorigenesis. Genes Dev 18:2095–2107